Available online at www.sciencedirect.com
ScienceDirect
Acta Materialia 55 (2007) 1965–1974
Acta MATERIALIA
www.actamat-journals.com

Ice-templated porous alumina structures

Sylvain Deville [1], Eduardo Saiz *, Antoni P. Tomsia

Materials Sciences Division, Lawrence Berkeley National Laboratory, Berkeley, CA 94720, USA

Received 16 August 2006; received in revised form 6 November 2006; accepted 7 November 2006
Available online 17 January 2007

Abstract

The formation of regular patterns is a common feature of many solidification processes involving cast materials. We describe here how regular patterns can be obtained in porous alumina by controlling the freezing of ceramic slurries followed by subsequent ice sublimation and sintering, leading to multilayered porous alumina structures with homogeneous and well-defined architecture. We discuss the relationships between the experimental results, the physics of ice, and the interaction between inert particles and the solidification front during directional freezing. The anisotropic interface kinetics of ice leads to numerous specific morphological features in the structure. The structures obtained here could have numerous applications, including ceramic filters and biomaterials, and could be the basis for dense multilayered composites after infiltration with a selected second phase.

Keywords: Porous ceramics; Multilayer; Freezing; Directional solidification; Physics of ice

1. Introduction

The formation of regular patterns is a common feature of many solidification processes, such as eutectic growth or unidirectional solidification of two-phase systems [1,2]. Control of the regularity and size of the patterns is often a key issue with regards to the final properties of the materials. Hence, particular attention has been paid to the control of solidification microstructures in the presence of inert particles [3], both theoretically and experimentally, as this technique has wide application in cast materials. The final microstructure is directly related to the shape and behavior of the solidification front, which can either engulf or repel the inert particles, such as ceramic particles in a solidifying metal.

Porous materials have attracted considerable attention as a new class of materials with a wide range of applications, from bone substitutes to parts for the automotive industry. In these materials, control of the size and morphology of the porosity is often the critical factor. Cellular ceramics can be engineered to combine several advantages inherent from their architecture [4]: they are lightweight, can have open or closed porosity (making them useful as insulators or filters), can withstand high temperatures, and can exhibit high specific strength, in particular in compression [5]. Typical processing methods include foam or wood replication [6–9], or direct foaming [10].

Of the many techniques used to prepare porous ceramics, freeze casting has not so far attracted much attention, although its simplicity certainly makes it appealing. The technique consists of freezing a liquid suspension (aqueous or otherwise), followed by sublimation of the frozen phase and subsequent sintering, leading to a porous structure with unidirectional channels in the case of unidirectional freezing, in which pores are a replica of the ice crystals [2] (in case of aqueous slurries). Although freeze casting has been applied to a wide variety of materials, such as alumina [11,12], hydroxyapatite [13], silicon nitride [14], NiO-YSZ [15] or polymeric materials [16], a proper and rational control of the microstructure morphology has not yet been achieved.

* Corresponding author. Tel.: +1 510 486 6202; fax: +1 510 486 4761.
E-mail address: Esaiz@lbl.gov (E. Saiz).
[1] Present address: Laboratoire de Synthèse et Fonctionnalisation des Céramiques, FRE2770, St Gobain CREE/CNRS, 84306 Cavaillon, France.

1359-6454/$30.00
doi:10.1016/j.actamat.2006.11.003

In freeze casting, the particles in suspension in the slurry are ejected from the moving solidification front and pile up between the growing columnar or lamellar ice, in a similar way (Fig. 1) to salt and biological organisms entrapped in brine channels in sea ice [17]. The variety of materials processed by freeze casting suggests that the underlying principles of the technique are not strongly dependent on the materials but rely more on physical rather than chemical interactions. The phenomenon is very similar to that of unidirectional solidification of cast materials and binary alloys, with ice playing the role of a fugitive second phase.

The porosity of the sintered materials is a replica of the original ice structure. Since the solidification is often directional, the porous channels run from the bottom to the top of the samples. In addition, the pores exhibit a very anisotropic morphology in the solidification plane. The final porosity content can be tuned by varying the particle content within the slurry, and the size of porosity is affected by the freezing kinetics [11]. More elaborate experimental setups have been designed to obtain radially oriented porosity [15]. The surface of the channels is covered by dendritic-like features, probably related to the morphology of the ice front, though no direct interpretation has been probed so far.

The motivation for this work was therefore to investigate freeze casting of ceramic slurries, and in particular the relationships between the freezing conditions and the final microstructures, for moderate to highly concentrated suspensions, and to interpret the phenomenon in terms of the interaction between the solidification front and the inert ceramic particles. We have discovered how under proper control of the freezing conditions, porous multilayered ceramics can be obtained [2]. The experimental setup was inspired by those used for the two-dimensional freezing experiments of low-concentration solutions [18,19], and modified for the processing of large three-dimensional samples, which may be characterized from a microstructural point of view. Alumina was used as a model material to investigate the relationships between the freezing conditions and the structure morphology. This inert oxide can be used to prepare stable and well-dispersed aqueous slurries with a wide range of solid contents.

2. Experimental techniques

Slurries were prepared by mixing distilled water with a small amount (1 wt.% of the powder) of ammonium polymethacrylate anionic dispersant (Darvan C, R.T. Vanderbilt Co., Norwalk, CT), an organic binder (polyvinyl alcohol, 2 wt.% of the powder) and the alumina powder (Ceralox SPA05, Ceralox Div., Condea Vista Co., Tucson, AZ) in various proportions. Slurries were ball-milled for 20 h with alumina balls and de-aired by stirring in a vacuum desiccator, until complete removal of air bubbles (typically 30 min). The powder used in the study (Fig. 2a) has a specific area of 8.1 $m^2 g^{-1}$ and an average grain size of 400 nm (manufacturer's data). A second powder with smaller particle size (<100 nm) (Fig. 2b) was also used; details can be found in Ref. [20].

Freezing of the slurries was done by pouring them into a Teflon mold (18 mm diameter, 30 mm long) with two copper rods on each side which were cooled using liquid nitro-

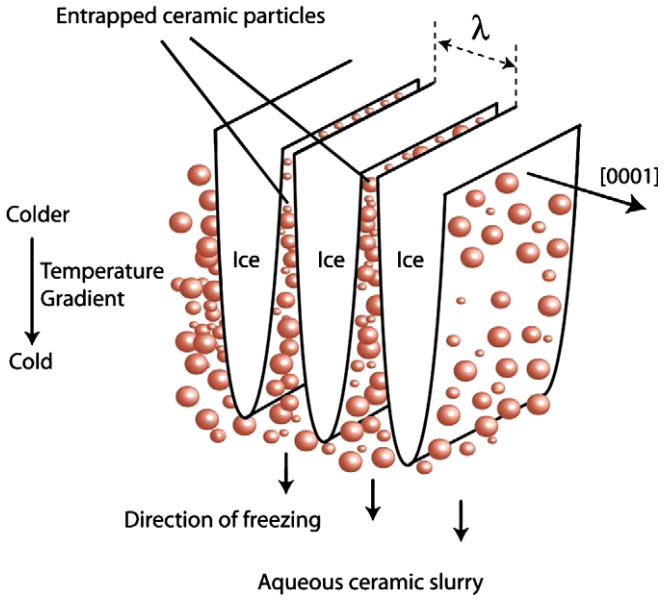

Fig. 1. Pattern formation and particle segregation during freeze casting of ceramic slurries. The ice platelets grow in a direction perpendicular to the *c*-axis of hexagonal ice. The wavelength of the structure is defined by λ.

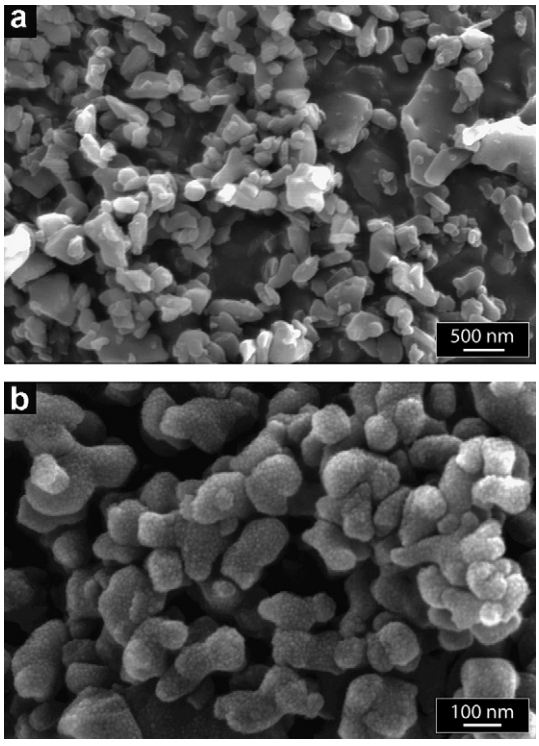

Fig. 2. SEM micrographs of the ceramic powders used in this study: (a) Ceralox SPA and (b) fine (~100 nm) alumina powder prepared according to Ref. [20].

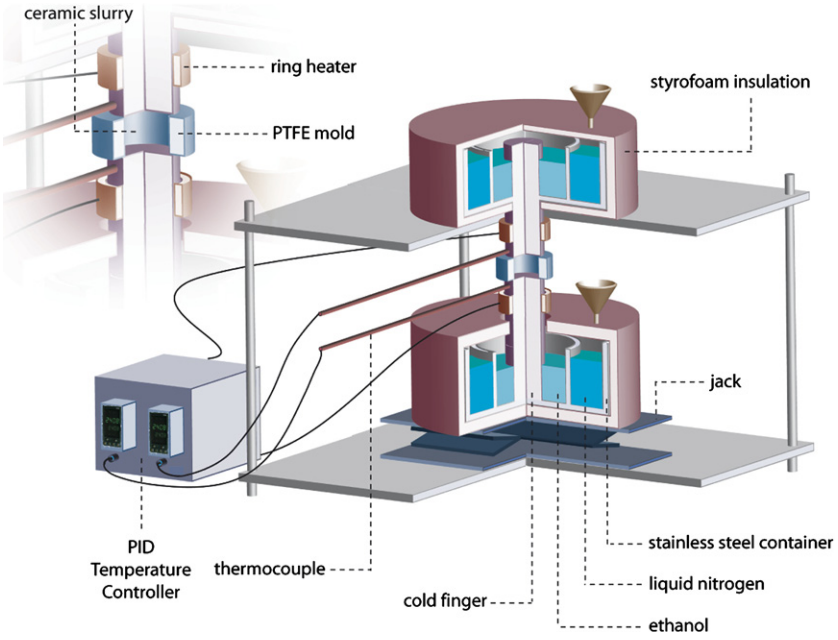

Fig. 3. Schematic of the experimental apparatus employed to directionally freeze the ceramic slurries while controlling the speed of the freezing front. The ceramic slurry is poured into a Teflon mold placed between two copper cold fingers whose temperature is controlled by liquid nitrogen baths and ring heaters.

gen [2] (Fig. 3). Freezing kinetics was controlled by heaters placed on the metallic rods and thermocouples placed on each side of the mold. Freezing occurred from bottom to top of the sample. Frozen samples were freeze-dried (Freeze Dryer 8, Labconco, Kansas City, MI) for 24 h. By adjusting both the temperature gradient and the cooling rate, a wide range of freezing conditions can be investigated. For low freezing rates, only the bottom cold finger was used. To reach higher freezing rates, a constant macroscopic temperature gradient was established using the two cold fingers cooled at the same rate. The average ice front velocity was estimated by measuring the time of freezing and dividing by the length of the frozen sample.

The green bodies thus produced were sintered in air for 2 h at 1500 °C, with heating and cooling rates of 5 °C min^{-1} (1216BL, CM Furnaces Inc., Bloomfield, NJ). The microstructure of the samples was analyzed by optical and environmental scanning electron microscopy (ESEM, S-4300SE/N, Hitachi, Pleasanton, CA) and their total porosity was derived from the apparent density, measured by Archimedes' method. The wavelength was measured in the top two-thirds of the sample where a constant thickness of the ceramic lamellae was reached. The wavelength was measured on lines perpendicular to the ceramic lamellae. More than 100 measurements per sample were performed.

3. Results

3.1. General features of the microstructure

If the slurry is partially quenched, i.e. poured over a cold finger maintained at a constant and negative temperature, the initial freezing is not steady. Although lamellae and channels are observed throughout the sample, their orientation over the cross section parallel to the ice front is completely random (Fig. 4a). Colonies of locally aligned pores are observed, but no long-range order is found.

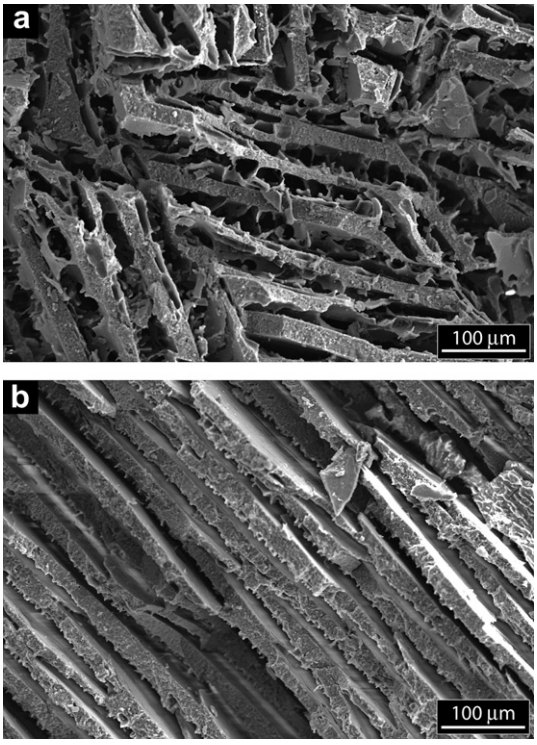

Fig. 4. SEM micrographs of the porous structure: (a) isotropic vs. (b) anisotropic microstructure. Cross-section parallel to ice front.

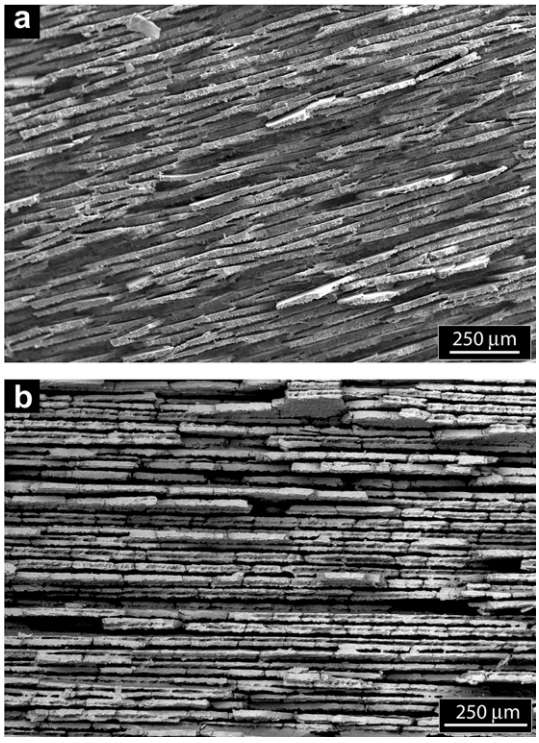

Fig. 5. SEM micrographs of homogeneous lamellar alumina cross-sections: (a) parallel to the ice front; (b) perpendicular to the ice front (ice growth from left to right).

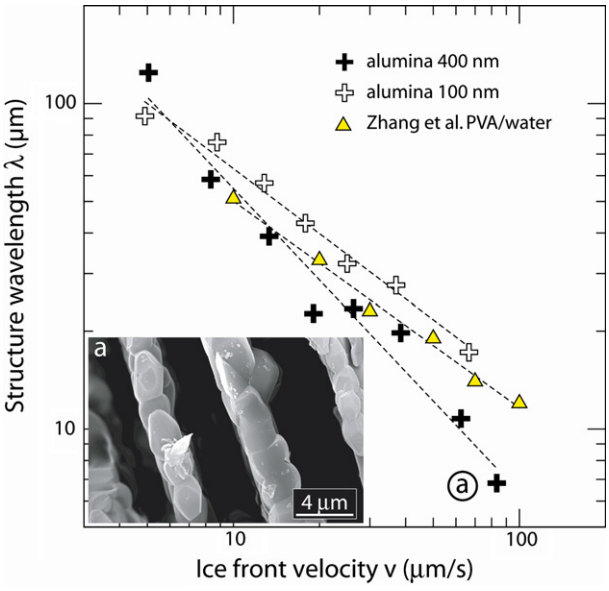

Fig. 7. Variation of structure wavelength vs. ice front velocity, for samples with 64% total porosity. The samples were frozen using only the bottom cold finger whose temperature was decreased at a constant rate (ranging between 0.1 and 10 °C min^{-1}). The only exception is the sample with ~2 µm lamellae thickness where both the top and bottom cold fingers were cooled at 2 °C min^{-1} in order to maintain a constant temperature gradient of ~1 °C cm^{-1}. The plots can be fitted with power laws, with exponents of 1 (alumina 400 nm) and 2/3 (alumina 100 nm and PVA/water). Comparison of the plots is discussed in the Section 4. A SEM micrograph of the sample with the smallest lamellae thickness achieved in this study is shown in the inset (a), cross-section parallel to the ice front. Lamellae thickness is ~2 µm. Each value on the graph is an average of >100 measurement of wall thickness in cross-section, using SEM micrographs. Error bars were not added to the graph here since on a log scale, error bars were smaller than the symbols.

Homogeneous freezing (i.e. cooling of the fingers at constant rate starting from room temperature) results in a more homogeneous ice nucleation [21], leading to a lamellar porous architecture (Fig. 4b), with long-range order, both in the parallel (Fig. 5a) and perpendicular (Fig. 5b) directions of the ice front. Channels run continuously from the bottom to the top of the sample, originating from a steady-state solidification front and previously continuous ice crystals. After sintering, the lamellae (Fig. 6) separating the lamellar channels are completely dense (Fig. 6d) with almost no visible residual porosity. The surface of the lamellae exhibits a particular topography, with dendritic-like features, 1–5 µm high, running in the direction of solidification (Fig. 6a and b). These features are homogeneous in size and distribution, but their relative size varies with the freezing conditions. Interestingly, after homogeneous freezing the dendritic surface relief covers only one side of the lamellae (compare Fig. 6a and c) while after quenching, dendrites are found on both sides (Fig. 4a). This particular feature is discussed in Section 4.3.

3.2. Influence of cooling rate on the microstructure

When the freezing kinetics is increased, i.e. the solidification front speed increases, the width of the channels and of

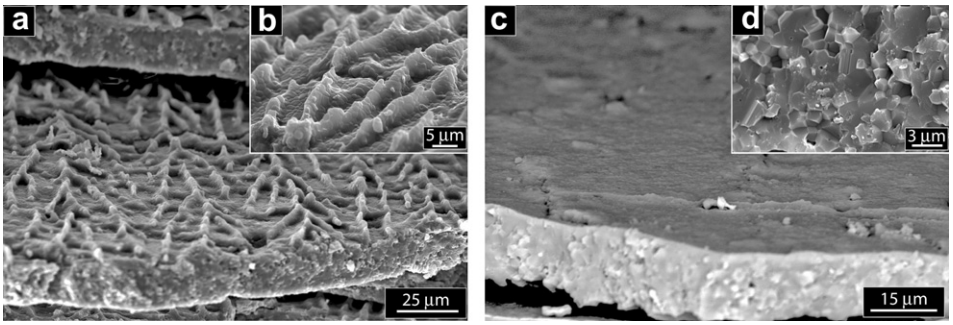

Fig. 6. SEM micrographs of lamellae surface features: (a) rough side with (b) details in insert and (c) smooth side. (d) Detail of the fracture surface of a lamella; the microstructure shows almost no residual porosity. The microstructure obtained after controlled solidification reveals that only one side of the lamellae is covered with dendritic-like features; the other side remains flat. This behavior is related to the anisotropic interface kinetics.

the lamellae is drastically affected. As shown in Fig. 7, the structure wavelength (defined in Fig. 1) can be varied over a wide range, from 7 to 130 μm, for a sample with 64% total porosity; the lamellae thickness in this case varies correspondingly from 2 to 44 μm (Fig. 7). The faster the freezing rate, the finer the microstructure. The empirical dependence (Fig. 7) of the wavelength (λ) on the speed of the ice front in the direction parallel to the temperature gradient (v) can be described by a simple power law ($\lambda \sim v^{-n}$). The dependence of n with the particle size brings some interesting observations. For the alumina with a 400 nm particle size, $n \approx 1$, but when the particle size decreases to ~100 nm, $n \approx 2/3$ as reported for a simple system with no particles (PVA/water [16]). The behavior of slurries with ceramic nanoparticles tends to closely resemble that of the simple system solute/water – a much simpler system to model. In addition, preliminary results [2] indicate that this variation might be dependent on the particle content, as pointed out by previous studies [3,22].

3.3. Influence of particle concentration in the slurry

The microstructure can also be modified by varying the concentration of the starting slurry (Fig. 8). Since the water initially present in the slurry is converted first into ice that is later eliminated to form the porosity, the pore content can be adjusted by tuning the slurry characteristics. The final porosity of the material is directly related to the volume of water in the suspension. Some limits are encountered. At low ceramic content, the green body becomes weaker and difficult to handle. Obtaining samples for ceramic contents lower than 40 wt.% is therefore difficult without increasing the binder content, but the features of the lamellar structure do not seem to be affected by the decrease of particle content. On the other hand, when the ceramic content is too high (>80 wt.%) (Fig. 8c), the lamellar structure is lost and the pores are not interconnected.

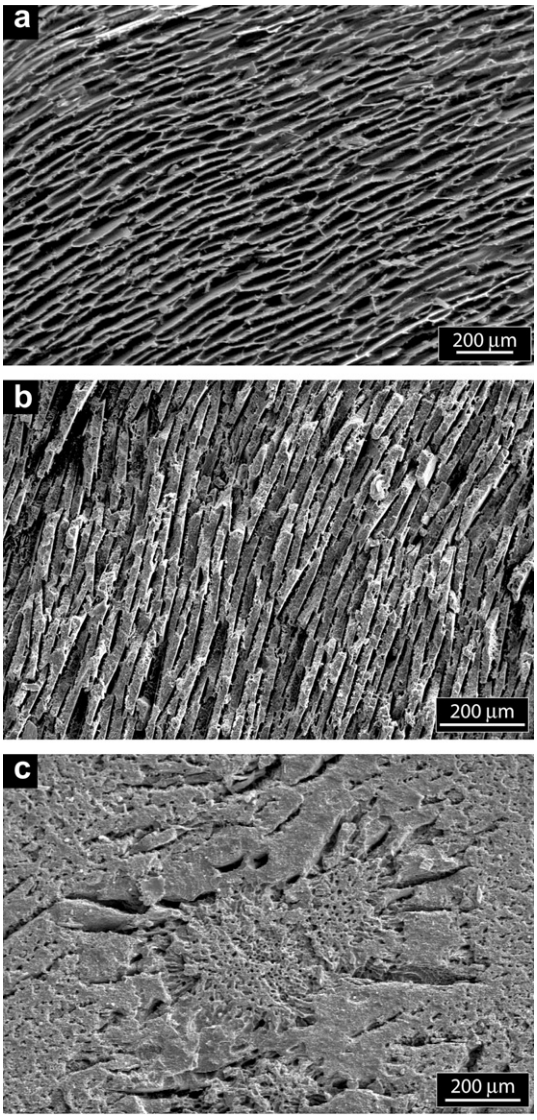

Fig. 8. SEM micrograph showing the influence of water content in the slurry on the microstructure. Cross-section parallel to ice front. Total porosity of: (a) 70%, (b) 40%, (c) 24%.

4. Discussion

4.1. Pattern formation mechanisms: the physics of ice and the interaction with inert particles

In order to obtain ceramic samples with a lamellar porous structure, two requirements must be satisfied:

1. The ceramic particles in suspension in the slurry must be rejected from the advancing solidification front and entrapped between the growing ice crystals.
2. The ice front must have a columnar or lamellar morphology.

Requirement (1) can be easily satisfied, and can be understood in terms of the interaction between an advancing solidification front and inert particles. Various analyses of this phenomenon in model suspensions [3,19,23] or biological or natural systems such as blood [24] or saltwater [25] have been published. All these fundamental investigations were made for suspensions with a very low concentration of particles, so that the interactions of particles with each other were not taken into account. The thermodynamic condition for a particle to be rejected by the solidification front is that there is an overall increase in free energy if the particle is engulfed by the solid:

$$\Delta\sigma = \sigma_{sp} - (\sigma_{lp} + \sigma_{sl}) > 0, \quad (1)$$

where σ_{sp}, σ_{lp} and σ_{sl} are the interfacial free energies associated with the solid–particle, liquid–particle and solid–liquid interface, respectively. For slow growth rates and in the absence of external forces, this thermodynamic criterion is often enough to predict if the particle is going to be entrapped or ejected by the solid [19,26]. However, for the solidification front to push the particles, a liquid film of sufficient thickness should exist between the solidification

front and the particle in order to maintain the transport of molecules towards the growing crystal. When the velocity of the front increases, the thickness of the film decreases. There is a critical velocity, v_c, for which this thickness is not enough to allow the necessary flow of molecules to keep the crystal growing behind the particle, which becomes then encapsulated by the solid. Several expressions have been derived for the critical velocity above which a particle will be entrapped. Most expressions define this critical velocity, v_c, as a function of the particle size, $R : v_c \propto \frac{1}{R}$ [24]. A simple model [16,19] based on the force balance at the particle/ice interface yields a critical ice front velocity for particle entrapment that can be written as:

$$v_c = \frac{\Delta\sigma d}{3\eta R}\left(\frac{a_0}{d}\right)^z, \quad (2)$$

where a_0 is the average intermolecular distance in the film, d is the overall thickness, η is the solution viscosity, R is the particle radius and z is an exponent that can vary from 1 to 5 depending on the specific model. The main problem with Eq. (2) is to estimate correctly d, z and $\Delta\sigma$. The behavior of nanoparticles such as those used here has never been investigated experimentally, and so the actual critical velocities can only be extrapolated from results obtained with larger particles. Typical critical velocities vary from 1 to 10 μm s^{-1} for particles with a diameter ranging from 1 to 10 μm (e.g. see Fig. 9 in Ref. [26]). Since the critical velocity is inversely proportional to the particle radius (Eq. (2)), it is likely to be very high (>100 μm s^{-1}) for submicrometer particles. A very rough estimate of the critical speed can also be obtained by disregarding the correction for the disjoining force of the particle ($z = 1$) and using some reasonable values for the other parameters ($R \approx 10^{-7}$m, $\Delta\sigma \sim \sigma_{sl} \sim 10^{-2}$ J m^{-2}, $a_0 \approx 10^{-8}$ m, $\eta \approx 10^{-2}$–10^{-3} Pa s); then $v_c \approx 1$–0.1 m s^{-1}. These comparisons support our observation that after the initial fast cooling (see Section 4.2) the alumina particles are always ejected by the ice front.

As far as requirement (2) is concerned, two possibilities need to be considered: the planar to columnar transition of

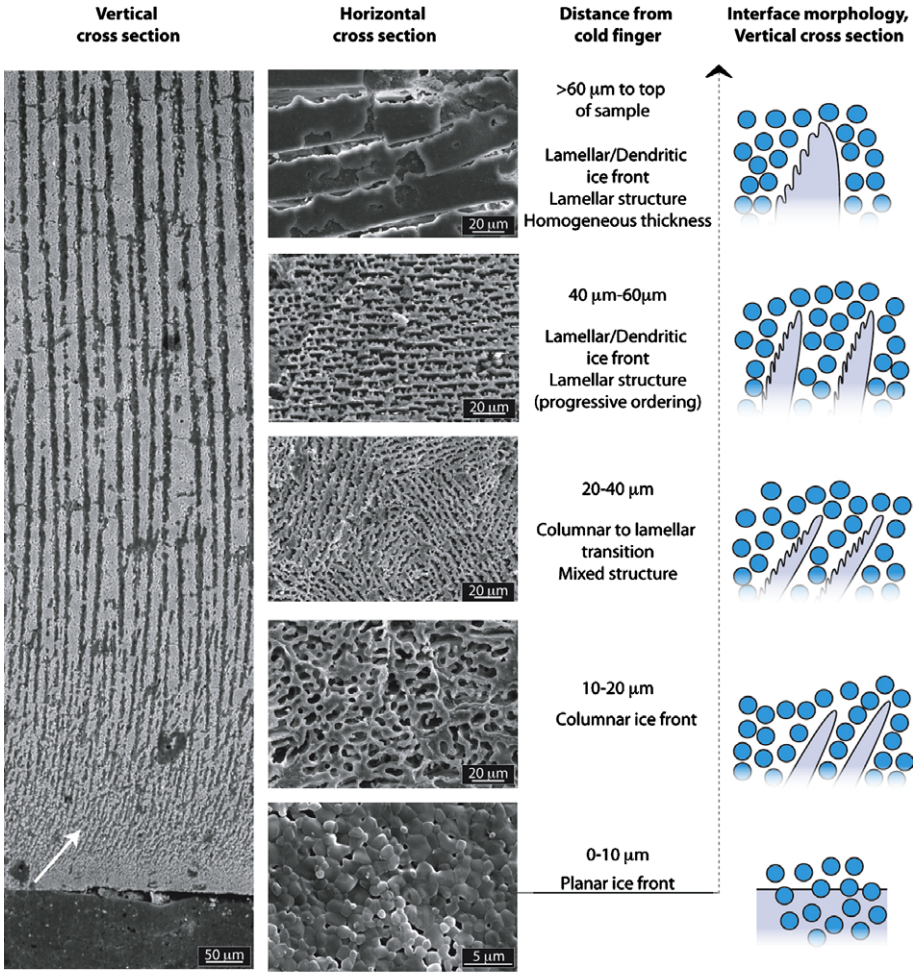

Fig. 9. SEM micrograph of the final microstructure and evolution of the ice front morphology. The black portion at the bottom of the sample is the epoxy that was used to embed the sample for cross-sectioning and polishing. It takes about 200–250 μm to reach homogeneous layer thickness; the layer thickens progressively with the height and then becomes constant. Tilting of the lamellae in the first frozen zone can be observed at the bottom of the micrograph (white arrow). The horizontal cross-sections (parallel to ice front) reveal the corresponding evolution of the porous structure and hence the interface morphology (depicted on the right).

the ice front can be generated by the constitutional supercooling ahead of the freezing front, or can be induced by the presence of particles. The crystal structure of ice is such that it has a very low solubility limit for impurities. Therefore, once an ice crystal is formed, any solute initially present in the water will be separated from this growing pure ice crystal and a local increase of solute concentration arises ahead of the ice front. If there is no equilibrium between the diffusion rate of the ejected solute and the rate of crystal growth, a concentration gradient builds up in the zone surrounding the ice front. The concentrated solute lowers locally the freezing point of the solution, leading to the formation of a constitutional supercooling zone in an unstable situation, which may eventually lead to the breakdown of the planar interface and the formation of a columnar interface, a phenomenon better known as a Mullins–Serkerka instability [27]. Further decrease in the ice front velocity (e.g. externally imposed) will result in a columnar to lamellar/dendritic transition. In our aqueous alumina slurries the chemical dispersant and polymeric binder added due to processing requirements are solutes ejected from the growing ice front that can provide the required constitutional supercooling and trigger the transition to the columnar or lamellar/dendritic ice front.

However, the breakdown of the planar interface may also be triggered by the presence of particles in the liquid [23]. This breakdown can occur for velocities below the threshold for the onset of a Mullins–Sekerka instability [23]. Observation of the microstructure (Fig. 9) suggests that the initial planar ice front is trapping the particles, resulting in a dense layer at the bottom of the sample. Afterwards, the formation of a cellular porous microstructure forms, indicating that the columnar ice front is rejecting the particles. This will suggest that initial freezing (the initial 10 μm) is very fast and the ice engulfs the particles. When the ice front velocity decreases below v_c, the rejected particles locally pin the ice front, triggering the transition from planar to columnar (Fig. 9). The ice front velocity parallel to the crystallographic c axis is 10^2–10^3 times lower than the velocity perpendicular to this axis. After the transition to columnar ice has occurred, ice platelets with a very large anisotropy can then be formed very fast with ice growing along the a-axes, while the thickness (along the c-axis) remains small. The freezing process is easier for crystals whose c-axes are perpendicular to the temperature gradient, such that growth along the gradient can occur in the a- or b-direction. The crystals with horizontal c-axes will therefore grow at the expense of the others and continue to grow upward, in an architecture composed of long vertical lamellar crystals with horizontal c-axes. In the final structures, the direction perpendicular to the lamellae thus corresponds to the original c-axis of the ice crystals [17]. A better understanding of the pattern formation in this case might be explained by incorporating the effect of the particles and the constitutional supercooling. Segregation of solutes will also affect the interfacial energies and in consequence the critical velocity for particle entrapment. Modeling of this complex phenomenon is well beyond the scope of this paper. However, in our preliminary experiments different solutes do not strongly affect the time of the planar to columnar transition, suggesting that the particles play a crucial role [28].

4.2. Initial gradient and morphological transition

In addition to the phenomenon triggering the morphological transition, some time is necessary for the freezing front to move from a planar to a columnar or lamellar/dendritic morphology. The transition is reflected in the final architecture of the porous structures, in the first frozen zone. A combination of parallel and perpendicular cross sections reveals the progressive transition and the intermediate stages (Fig. 9). Initial freezing is very fast and then the velocity of the liquid front decreases rapidly until it reaches a steady state with an approximate constant value. Consequently, the first frozen zone reveals a planar ice front at which the alumina particles have become entrapped. The interface then moves progressively to a columnar and eventually lamellar morphology, with a progressive ordering of the lamellae. A steady state is eventually reached and ice crystals become continuous, running through the entire sample, with a constant thickness. It is worth pointing out here that these observations allow us to rationalize previous results in the literature, where morphological transitions during freezing were observed but not explained [29,30].

4.3. Anisotropy of interface kinetics

The thickness of the ice crystals is strongly dependent on the speed of the solidification front. Faster freezing velocities result in larger supercooling in front of the growing crystals that will influence the crystal thickness. In addition, as faster growth is imposed in the direction of the temperature gradient, lateral growth along the c-axis is increasingly limited, resulting in thinner lamellae. The results suggest that addition of particles above some critical size of few hundred nanometers will also affect the relative kinetics of crystal growth.

In a two-dimensional cross section perpendicular to the ice lamellae and the freezing front, it is possible to define two growth directions for the ice crystals: parallel to the temperature gradient (with a growth rate v), and along the preferred growth direction (in the sense of interfacial energies), with a growth rate v_p. These directions can be different, which may result in tilted crystal growth (Fig. 10). The balance between imposed and preferred growth results in two characteristic phenomena: the formation of dendrites on the lamellar ice crystals and tilting of the crystals at very fast cooling rates [31,32]. The freezing kinetics depends on a myriad of factors (heat of fusion, convection in the suspension, thermal diffusivities, etc.) and is an extremely complex phenomenon to model. However, the ratio v_p/v is strongly dependent on the magnitude

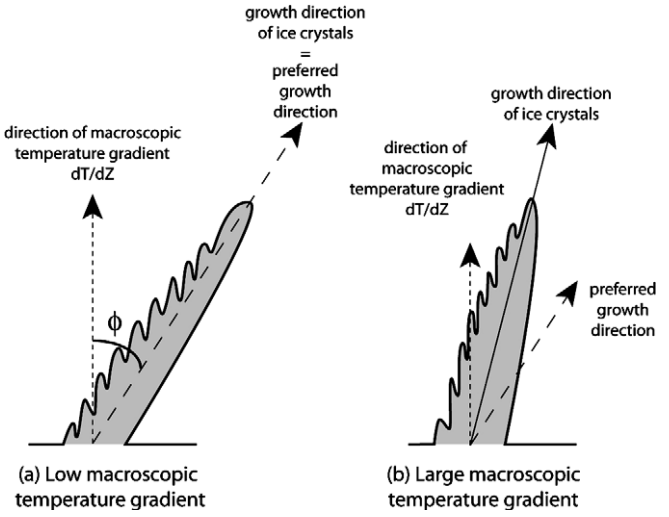

Fig. 10. Growth direction of ice crystals and relationships with imposed macroscopic temperature gradient and preferred growth direction.

of the temperature gradient: $(T_1–T_2)/L$, where $T_1(t)$ and $T_2(t)$ are the time-dependent temperatures of the top and the bottom cold finger and L is the length of the mold, which influences the growth kinetics. Two main regimes can be observed in our experiments.

During steady-state growth, the temperature gradient and the driving force for directional growth are relatively large and consequently $v \gg v_p$. The ice crystals grow tilted just a few degrees with respect to the direction of the temperature gradient, while in one side of the crystals small dendrites a few micrometers in height aligned with the direction of the gradient form. Due to the growth pattern these dendrites are found only on one side of the lamellae (Fig. 6a), the other side being flat (Fig. 6c). The dendrites are observed independently of the initial powder content within the slurry. The ceramic particles entrapped in the channels between the converging secondary fronts of the ice cells, such as the surface dendrites, generate the observed roughness on one side of the ceramic lamellae, while the other side remains flat after removing the ice [25]. Modifying the topography of the wall surface will therefore involve controlling the dendritic ice morphology.

As the temperature gradient decreases, the dependence on the imposed growth direction becomes less marked and when the temperature gradient direction and the preferred growth direction (due to crystalline anisotropy) are different, anisotropic interface kinetics may play a role. A decrease in the temperature gradient is accompanied by a decrease in the driving force for directional growth and consequently in v/v_p. The macroscopic result of this mismatch is an increasing tilt of the ice crystals (and hence of the resulting ceramic lamellae, Fig. 11). The overall tilting of the cells depends on the magnitude of the anisotropic interface kinetic effect. This behavior is observed in the first frozen zone of samples prepared using only the bottom cold finger. When this zone forms, the macroscopic gradient is still relatively small ($<1\ °C\ mm^{-1}$) and the first-formed lamellae exhibit a strong tilting (Fig. 9, vertical cross-section), similar to that observed in Fig. 11. As the temperature of the bottom cold finger decreases, the gradient increases, and a steady freezing state is progressively reached and tilting becomes less marked; the ice crystals become closely aligned along the direction of the temperature gradient.

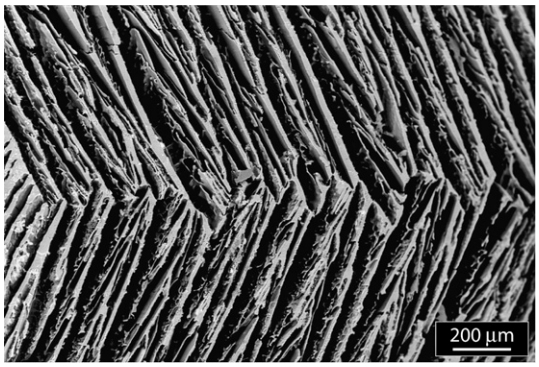

Fig. 11. SEM micrograph showing tilting of the lamellae due to the effect of anisotropic interface kinetics. Cross-section perpendicular to ice front. In this case, the sample was frozen very fast using the top and bottom cold fingers to set a very small gradient, so that the crystals started on both sides almost simultaneously and joined in the middle of the sample. The tilting (15–20°) is clearly visible.

4.4. Ceramic bridges

Another microstructural feature are the translamellar ceramic bridges (e.g. Fig. 12), which are observed only for highly concentrated slurries. In the sintered porous structures, these numerous fine features, with often-tortuous morphologies, locally bridge the gap between two adjacent lamellae. The morphology of these features is very different to that of the dendrites (see Fig. 6b) covering the ceramic lamellae, suggesting another formation mechanism. We propose here that they might be formed because of the specific conditions encountered during the slow freezing of highly concentrated solutions. The interaction of inert particles and a moving solidification front has been investigated for suspensions with low particle content. In

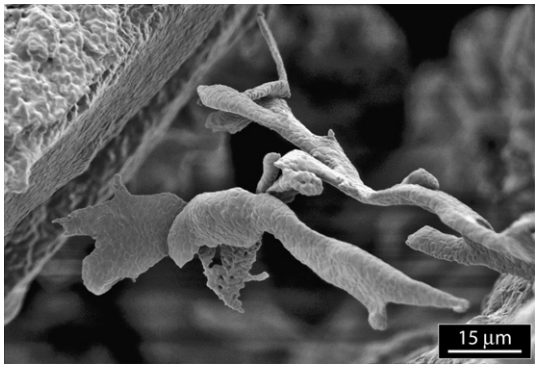

Fig. 12. SEM micrograph of ceramic bridges observed for slow freezing of highly concentrated slurries.

such a case, the interaction between particles is not taken into account, which considerably simplifies the associated modelling. In the case of highly concentrated solutions, the particle–particle interactions can no longer be ignored. Eventually, these interactions may greatly affect the pattern formation mechanisms. It has previously been shown that the particles themselves may induce morphological transitions, such as dendrite tip splitting or healing, during growth before being captured [3]. Ceramic bridges between lamellae may arise from local ice crystal tip splitting and engulfment of particle agglomerates created by particles repelled from the ice–water interface and subsequent tip healing. Depending on the magnitude of tip splitting/healing, the entrapped ceramic particles might not completely bridge the gap.

4.5. Controlling the structure

Freeze casting is based on a physical process, the formation of ice, and the results described here for alumina can be extrapolated to a wide range of materials, opening the path towards numerous applications. Recent works have shown how this process can be adapted to the fabrication of porous polymer or hydroxyapatite scaffolds for tissue engineering [13,16] or as the base for the fabrication of hybrid materials [33] or multilayered nacre-like composites after subsequent infiltration with a suitable second phase [2].

From the previous discussion, it is clear that the relationship between ice front velocity and structure wavelength is extremely complex to describe via a simple analytical model. The investigated system is a multicomponent one, combining the effect of the particle/ice front interactions and solute segregation. The structure wavelength (or ice crystal radius) will therefore depend on a large number of factors, including the freezing rate (or ice front velocity); the interfacial free energy between the particles, the water and the ice front; the particles size, distribution and content; the interactions of the particles with themselves; the anisotropic effects of the surface tension of ice; the buoyancy forces acting on the particles; the viscosity of the slurry; the diffusion of the solute away from the interface; the latent heat diffusion; and so on. Nevertheless, some trends, summarized in Fig. 13, emerge from our studies.

The empirical dependence (Fig. 7) of the structure wavelength on the particle size enables some interesting observations. It seems that when the particle size becomes negligible compared to the ice tip radius (~100 nm in our experiment), the behavior of the multicomponent system approximates to that of a simple aqueous solution, which can be predicted by linear stability analysis. Extending this approach to include structures with thin lamellae will involve two conflicting behaviors. On the other hand, the lamellae thickness cannot be made thinner than the particle size, but by using nanoparticles the exponent n, which marks the dependence of the wavelength with the vertical velocity of the ice front decreases, and thicker lamellae are

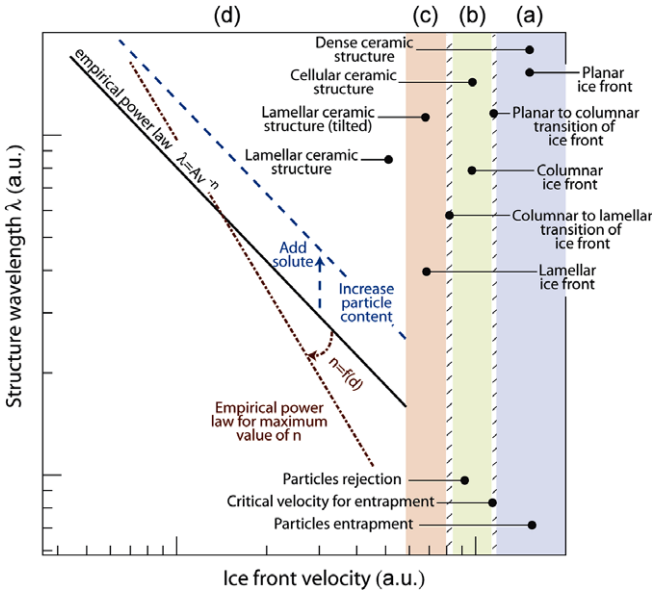

Fig. 13. Strategies and limits for controlling the structure: schematic plot of wavelength vs. ice front velocity. The exponent n of the empirical law is dependent on the particle size d, though the function $n = f(d)$ is not monotonic; an optimum value of d is encountered where the exponent n is maximum. Very fast cooling rates, region (a), will result in the ice front trapping the particles and the formation of a dense material, such as the one observed in the bottom layer of Fig. 9. When the velocity is decreased below the critical value for particle entrapment, v_c, the particles are expelled from the growing ice but if the speeds are fast enough the ice will grow with a columnar microstructure, region (b). Slower velocities will result in the formation of lamellar ice. However, if the velocity is still fast or, equivalently, the gradient in temperature small enough, the balance between the preferential growth direction and the gradient direction will result in the growth of lamellae tilted with respect to the later, region (c). As the velocity decreases (or the gradient increases) the lamellae will align with the direction of the temperature gradient, region (d).

obtained. A compromise has to be found in terms of particle size for reducing the lamellae thickness. There seems to be an optimum particle size at which the structure wavelength reaches a minimum (and hence the exponent n a maximum). Our preliminary results using different additives [28] suggest that these do not have a strong effect on the dependence of the wall thickness on freezing rate. Investigations with additional well-controlled powders will be needed to clarify these points and identify this optimum.

5. Conclusions

Based on our experimental investigations of the controlled freezing of moderate to highly concentrated ceramic aqueous suspensions, the following conclusions can be drawn:

1. Homogeneous lamellar porous structures can arise from the controlled freezing of ceramic slurries, followed by sublimation of the ice and sintering of the porous green bodies. The porosity is open, unidirectional and homogeneous throughout the whole sample.

2. The pattern formation mechanisms can be qualitatively understood by the application of the simple principles of the physics of ice, and the interaction of inert particles with the solidification front.
3. The morphology of the porous structures, i.e. the content, dimensions, shape and orientation of porosity, can be controlled to some extent by the initial slurry compositions and the freezing conditions. For highly concentrated solutions, the particle–particle interactions should probably be taken into account to explain the experimental results, in particular the formation of ceramic bridges between lamellae.

Acknowledgement

This work was supported by the Director, Office of Science, Office of Basic Energy Sciences, Materials Sciences and Engineering Division, of the U.S. Department of Energy under Contract No. DE-AC02-05CH11231.

References

[1] Hunt JD. Mater Sci Technol 1999;15(1):9–14.
[2] Deville S, Saiz E, Nalla RK, Tomsia A. Science 2006;311:515–8.
[3] Sekhar JA, Trivedi R. Mater Sci Eng A 1991;147A:9–21.
[4] Green DJ, Colombo R. MRS Bull 2003;28(4):296–300.
[5] Gibson LJ. MRS Bull 2003;28(4):270–1.
[6] Herzog A, Klingner R, Vogt U, Graule T. J Am Ceram Soc 2004;87(5):784–93.
[7] Sieber H, Hoffmann C, Kaindl A, Greil P. Adv Eng Mater 2000;2(3):105–9.
[8] Sun B, Fan T, Zhang D. J Porous Mater 2002;9(4):275–7.
[9] Cao J, Rambo CR, Sieber H. J Porous Mater 2004;11(3):163–72.
[10] Sepulveda P, Binner JGP. J Eur Ceram Soc 1999;19(12):2059–66.
[11] Fukasawa T, Deng ZY, Ando M, Ohji T, Goto Y. J Mater Sci 2001;36(10):2523–7.
[12] Araki K, Halloran JW. J Am Ceram Soc 2005;88(5):1108–14.
[13] Deville S, Saiz E, Tomsia A. Biomaterials 2006;27(32):5480–9.
[14] Fukasawa T, Deng ZY, Ando M, Ohji T, Kanzaki S. J Am Ceram Soc 2002;85(9):2151–5.
[15] Moon JW, Hwang HJ, Awano M, Maeda K. Mater Lett 2003;57(8):1428–34.
[16] Zhang HF, Hussain I, Brust M, Butler MF, Rannard SP, Cooper AI. Nat Mater 2005;4(10):787–93.
[17] Petrenko VF, Whitworth RW. Physics of ice. Oxford: Oxford University Press; 2002.
[18] Esaka H, Kurz W. J Cryst Growth 1985;72(3):578–84.
[19] Korber C, Rau G, Cosman MD, Cravalho EG. J Cryst Growth 1985;72:649–62.
[20] Morinaga K, Torikai T, Nakagawa K, Fujino S. Acta Mater 2000;48(18–19):4735–41.
[21] Schoof H, Apel J, Heschel I, Rau G. J Biomed Mater Res 2001;58(4):352–7.
[22] Shanti NO, Araki K, Halloran JW. J Am Ceram Soc 2006;89(8):2444–7.
[23] Hadji L. Eur Phys J B 2004;37(1):85–9.
[24] Ishiguro H, Rubinsky B. Cryobiology 1994;31:483–500.
[25] Worster MG, Wettlaufer JS. J Phys Chem B 1997;101(32):6132–6.
[26] Asthana R, Tewari SN. J Mater Sci 1993;28:5414–25.
[27] Mullins WW, Sekerka RF. J Appl Phys 1964;35(2):444–51.
[28] Deville S. Unpublished results.
[29] Zmora S, Glicklis R, Cohen S. Biomaterials 2002;23(20):4087–94.
[30] Madihally SV, Matthew HWT. Biomaterials 1999;20(12):1133–42.
[31] Young GW, Davis SH, Brattkus K. J Cryst Growth 1987;83:560–71.
[32] Nagashima K, Furukawa Y. J Cryst Growth 1997;171(3-4):577–85.
[33] Gutiérrez MC, Jobbágy M, Rapún N, Ferrer ML, del Monte F. Adv Mater 2006;18(9):1137–40.